Journal of Magnetic Resonance 209 (2011) 69–74

Contents lists available at ScienceDirect

Journal of Magnetic Resonance

journal homepage: www.elsevier.com/locate/jmr

Integrated refocused virtual ESEEM: Detection of nuclear transition spectra without dead time and blind spots

Andrei V. Astashkin *

University of Arizona, Department of Chemistry and Biochemistry, Tucson, AZ 85721, USA

ARTICLE INFO

Article history:
Received 28 September 2010
Revised 4 January 2011
Available online 8 January 2011

Keywords:
ESEEM spectroscopy
Refocused virtual ESEEM
ESE
Pulsed EPR

ABSTRACT

General expressions describing the refocused stimulated (RS) and refocused virtual (RV) electron spin echo envelope modulations (ESEEM) generated with the same basic four-pulse sequence are derived. It is shown that integration of the 3D time domain trace over the two "low-resolution" time intervals (those between the first and second and between the third and fourth microwave pulses) results in a dead time-free 1D ESEEM trace in the "high-resolution" dimension (i.e., the time interval between the second and third microwave pulses) that only contains harmonics with the fundamental frequencies of nuclear transitions. The practical implementation of the integrated RS ESEEM requires pulse swapping, which leads to unrecoverable distortions in the ESEEM traces and the resulting spectra. The integrated RV ESEEM is free from such distortions and represents a robust practical technique for obtaining dead time- and blind spots-free spectra of nuclear transitions, without homonuclear combination lines. As an application example, the integrated RV ESEEM was used to obtain the spectrum of a strongly-coupled proton of the OH ligand of the Mo(V) active center of the low-pH form of the molybdoenzyme sulfite oxidase.

1. Introduction

Electron spin echo (ESE) envelope modulation (ESEEM) spectroscopy is a generic name for a multitude of pulsed electron paramagnetic resonance (EPR) techniques used to obtain high-resolution spectra of magnetic nuclei interacting with the unpaired electron, and to determine the hyperfine and nuclear quadrupole interactions (*hfi* and *nqi*, respectively) of those nuclei [1,2]. During the five decades after the first ESEEM observations by the simplest two-pulse technique [3–5], the field of ESEEM methodology has seen active development, with numerous more complex techniques being implemented. The current list of only those techniques employing hard microwave (mw) pulses and used in routine practical measurements includes the primary (two-pulse) [6], stimulated (three-pulse) [6,7], four-pulse [8,9], hyperfine sublevel correlation (HYSCORE) [10], and refocused primary (RP) ESEEM [11]. These techniques have somewhat different properties, which include the presence or absence of combination harmonics, dimensionality (1D, 2D, *etc.*), achievable resolution in ESEEM spectra (high resolution determined by the longitudinal relaxation rate, or low resolution determined by the transverse relaxation rate), dead time, *etc.* The set of properties of a given ESEEM technique makes it better suited for solving some specific types of spectroscopic problems and less suitable for other types. For example, the anisotropic *hfi* and weak *nqi* in the weak *hfi* regime ($\nu_I > A/2$, where ν_I is the nuclear Zeeman frequency and A is the diagonal part of the *hfi*) are usually most easily estimated from the sum combination feature in the spectra of two- or four-pulse ESEEM [12–15], while the isotropic *hfi* can be estimated from the fundamental lines in the spectra generated by any of the ESEEM techniques. Both *hfi* and intermediate *nqi* under the Zeeman – *hfi* cancellation conditions ($\nu_I \sim A/2$) are most readily estimated from the fundamental lines [16], and therefore the three-pulse ESEEM is often used to obtain the spectra of ^{14}N in such situations [17–23]. The case of strong *nqi* ($e^2Qq/h \gg \nu_I \pm A/2$) is most easily addressed using HYSCORE [10,24–26], and the same technique is generally used to disentangle complex crowded spectra contributed to by several nuclei.

While HYSCORE is probably the most powerful and versatile ESEEM technique, it has a disadvantage of being rather time-consuming because (1) the data acquisition time is proportional to N^2, where N is the number of data points in one dimension of the $N \times N$ 2D data set and (2) the spectra are distorted by the presence of blind spots that depend on the time interval between the first and second mw pulses, τ. To minimize the loss of information due to the blind spots, typically, the HYSCORE spectra at several intervals τ have to be obtained, which increases the overall duration of the experiment [27]. Another disadvantage originates from the fact that the detected ESE signal in HYSCORE is composite (contributed to by the inverted and non-inverted stimulated ESE signals), and the ESEEM amplitude is difficult to interpret in terms

* Fax: +1 520 621 8407.
E-mail address: andrei@u.arizona.edu

1090-7807/$ - see front matter © 2011 Elsevier Inc. All rights reserved.
doi:10.1016/j.jmr.2011.01.001

of the number of nuclei and the interaction strength [28]. Therefore, 1D techniques are still very much in use, and development of new ESEEM techniques with desired properties is still in progress.

The spectral blind spots are a common feature of ESEEM experiments where only part of the time intervals are swept to produce an ESEEM trace, while other time intervals are used as fixed parameters. Such an approach is typical for stimulated ESEEM and HYSCORE (in both cases the time interval τ between the first two pulses is used as a parameter), and in order to deal with the blind spots, the amplitude Fourier transformation (FT) spectra are often obtained for several intervals τ and either considered as a set or added together. A sum of the amplitude FT spectra obtained for a sufficiently large set of τ values results in a nearly undistorted amplitude FT spectrum with meaningful relative amplitudes of various spectral features [27].

As an alternative to the summation of the amplitude FT spectra, it has been recently realized that for some intrinsically 2D techniques an integration over the parameter time interval results in a 1D ESEEM trace with practically zero dead time (the residual dead time is about the mw pulse length) and uniform scaling of the harmonic amplitudes (no blind spots in the spectrum). All of the harmonics in such a trace are phased as $\pm\cos(\omega_t)$ ("+" for fundamental harmonics and "−" for homonuclear combination harmonics), and the cosine FT spectrum phased to the time origin is not distorted by the dead time-related side lobes and permits easy identification of fundamental and combination lines. The examples of such an approach are the τ-integrated RP ESEEM [11,14] and τ-integrated four-pulse ESEEM [11,15]. Similar technique implemented in τ-integrated stimulated ESEEM [29] with pulse swapping [30] eliminates the spectral blind spots, although the dead time is still determined by the resonator ringing.

Since the τ-integration of stimulated ESEEM fails to completely eliminate the dead time, we were interested in finding an alternative ESEEM technique that would be dead time- and blind spots-free, but retain the essential property of the stimulated ESEEM of only containing harmonics with the fundamental nuclear transition frequencies phased as $\cos(\omega_t)$. As simplest possible candidates, we consider in this work two ESEEM techniques, which are intrinsically 3D, but whose dimensionality is reduced to effective 1D by integration over two of the time intervals. These techniques are based on refocused stimulated (RS) and refocused virtual (RV) ESE signals generated by the pulse sequence shown in Fig. 1. While the stimulated echo (SE in Fig. 1) is a quite familiar and much used ESE signal, the virtual echo (VE in Fig. 1) deserves a comment. As noted by Bloom [31], this is not a real observable echo signal, but the magnetization after the third pulse behaves in every way as if this signal actually existed. The fourth pulse refocuses the magnetization diverging after the SE and VE signals to form the corresponding refocused echoes (RSE and RVE in Fig. 1), both of which are observable. Although the RS and RV ESE signals were used in pulsed electron-nuclear double resonance (ENDOR) [18,32] and relaxation-induced dipolar modulation enhancement (RIDME) [33–35] measurements, the corresponding ESEEM has never been utilized in practical experiments or even analyzed theoretically.

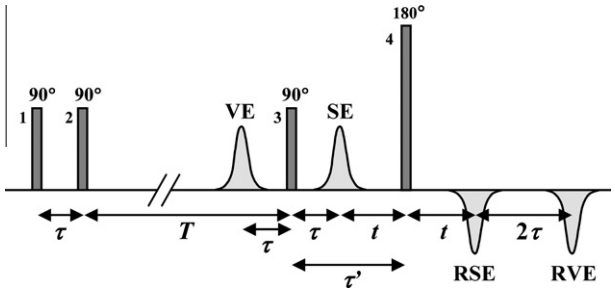

Fig. 1. The pulse sequence for generating the RS and RV ESEEM signals. Only the essential ESE signals are shown. The labels "SE", "VE", "RSE" and "RVE" denote stimulated, virtual, refocused stimulated, and refocused virtual ESE signals, respectively. The 1–2, 2–3 and 3–4 inter-pulse time intervals are, respectively, τ, T and τ'. The time interval $t = \tau' - \tau$ is between the SE signal and the fourth mw pulse.

The analysis performed in this work shows that the RS and RV ESEEM data sets integrated over two of the time intervals (τ and t in Fig. 1) represent 1D traces showing oscillations in the T dimension containing only the fundamental harmonics. While both techniques can be implemented in such a way as to have nearly zero dead time, the RS ESEEM requires pulse swapping, which introduces distortions due to the unavoidable collapse of the ESE signal when the swapped mw pulses overlap. The RV ESEEM is free from such distortions and should be preferred over the RS ESEEM technique. As an example, the integrated RV ESEEM is applied in this work to obtain a spectrum of fundamental lines of strongly-coupled protons in the molybdenum-containing enzyme sulfite oxidase (SO).

2. Experimental

The experiments have been performed on a homemade K_a-band (26–40 GHz) pulsed EPR spectrometer [36] at the temperature of about 21 K. The sample of the low-pH form of recombinant human SO [37] used for the demonstration of the integrated RV ESEEM was kindly made available for this study by Prof. J.H. Enemark. The details of sample preparation are described elsewhere [38].

3. Results and discussion

3.1. General expressions

In this work we have researched the possibility that the RS or RV ESEEM can be used to obtain the spectra of fundamental lines of nuclear transitions that are free from the dead time artifacts, and phase properly and uniformly in the cosine FT spectra. The pulse sequence for both techniques is the same, and it is shown in Fig. 1. The general analytical expressions were obtained assuming ideal mw pulses and using the density matrix formalism as laid out by Mims [6]. In a high temperature approximation, the general expressions for the RS and RV ESEEM are as follows:

$$V_{RS} = \mathrm{Re} \sum_{i,j,k,l,m,n} C_M \tilde{t}_{\alpha mi} \tilde{t}_{\beta nj} \tilde{\tau}_{\alpha mk} \tilde{\tau}_{\beta lj} (\tilde{T}_{\alpha mk} + \tilde{T}_{\beta lj}) \quad (1)$$

$$V_{RV} = \mathrm{Re} \sum_{i,j,k,l,m,n} C_M \tilde{t}_{\alpha mi} \tilde{t}_{\beta nj} \tilde{\tau}_{\alpha mi} \tilde{\tau}_{\beta nj} (\tilde{T}_{\alpha mk} \tilde{\tau}_{\alpha mi} \tilde{\tau}_{\beta nl} + \tilde{T}_{\beta lj} \tilde{\tau}_{\alpha ki} \tilde{\tau}_{\beta nj}) \quad (2)$$

where

$$\begin{aligned} C_M &= M_{ij} M^+_{jk} M_{kl} M^+_{lm} M_{mn} M^+_{ni} \\ \tilde{\tau}_{\alpha(\beta)km} &= \exp(i\omega_{\alpha(\beta)km}\tau) \\ \tilde{t}_{\alpha(\beta)km} &= \exp(i\omega_{\alpha(\beta)km}t) \\ \tilde{T}_{\alpha(\beta)km} &= \exp(i\omega_{\alpha(\beta)km}T) \end{aligned} \quad (3)$$

and τ, t, and T are the time intervals shown in Fig. 1. The pulse propagator matrices **M** are composed of the matrix elements of transition operator S_X: $M_{ij} = \langle\psi_{\alpha i}|S_X|\psi_{\beta i}\rangle$, and $\omega_{\alpha(\beta)} = 2\pi\nu_{\alpha(\beta)}$ are the nuclear transition frequencies within the α and β electron spin manifolds.

Eqs. (1) and (2) describe 3D data sets, τ *vs.* t *vs.* T. In practical terms, the three dimensions are not equivalent, with τ and t being the "low-resolution" dimensions, where the ESE signal decay is determined by the electronic transverse relaxation rate, and T

being the "high-resolution" dimension, where the ESE signal decay is determined by the longitudinal relaxation. This fact, as well as the number of dimensions greater than two, limit the possible application of RS and RV ESEEM as multi-dimensional techniques. On the other hand, as shown below, they have several very useful properties if implemented as 1D techniques.

One of the practical methods to obtain a 1D data set out of a multidimensional data set consists in integration over all but one dimensions. This approach was successfully implemented in τ-integrated RP ESEEM [11,14], τ-integrated four-pulse ESEEM [11,15], and τ-integrated stimulated ESEEM [29], where the 1D data sets were obtained from 2D data sets by integration over the time interval between the first two mw pulses, τ. Similar approach can be applied to the RS and RV ESEEM in order to obtain a 1D ESEEM as a function of the "high-resolution" coordinate, T. As a preliminary step, we rewrite Eqs. (1) and (2) as:

$$V_{RS} = V_{RSo}(\tau,t,T) + \mathrm{Re}\sum_{m=i,j=n=l,k} C_M(\widetilde{T}_{\alpha mk}\tilde{\tau}_{\alpha mk} + \tilde{\tau}_{\alpha mk}) + \mathrm{Re}\sum_{m=i=k,j=n,l} C_M(\widetilde{T}_{\beta lj}\tilde{\tau}_{\beta lj} + \tilde{\tau}_{\beta lj}) \quad (4)$$

$$V_{RV} = V_{RVo}(\tau,t,T) + \mathrm{Re}\sum_{m=i,j=n=l,k} C_M(\widetilde{T}_{\alpha mk} + \tilde{\tau}_{\alpha km}) + \mathrm{Re}\sum_{m=i=k,j=n,l} C_M(\widetilde{T}_{\beta lj} + \tilde{\tau}_{\beta jl}) \quad (5)$$

where $V_{RSo}(\tau, t, T)$ and $V_{RVo}(\tau, t, T)$ contain all of the terms not included into the explicit sums. These terms contain harmonics $\cos(\omega_\tau\tau + \omega_t t + \omega_T T)$ with $\omega_\tau \neq 0$ or $\omega_t \neq 0$.

An unconditional integration of V_{RS} (Eq. (4)) over τ and t obviously results in averaging out the oscillations in the T dimension:

$$V_{iRS} \propto \mathrm{Re}\sum_{m=i=k,j=n=l} C_M = \mathrm{const} \quad (6)$$

However, considering $T' \equiv \tau + T$ in Eq. (4) as an independent time variable, one can perform the integration over τ subject to the condition T' = const. Under this condition, the integration over τ and t results in:

$$V_{iRS} = \mathrm{Re}\sum_{m=i,j=n=l,k} C_M\widetilde{T}'_{\alpha mk} + \mathrm{Re}\sum_{m=i=k,j=n,l} C_M\widetilde{T}'_{\beta lj} \quad (7)$$

where $\widetilde{T}'_{\alpha(\beta)ik} = \exp(i\omega_{\alpha(\beta)ik}T')$. The situation with integration of V_{RS} over τ is thus similar to that in the τ-integrated stimulated ESEEM [29], where the condition T' = const is also essential for preserving the oscillation in the T dimension.

For V_{RV}, the unconditional integration of Eq. (5) over τ and t results in:

$$V_{iRV} = \mathrm{Re}\sum_{m=i,j=n=l,k} C_M\widetilde{T}_{\alpha mk} + \mathrm{Re}\sum_{m=i=k,j=n,l} C_M\widetilde{T}_{\beta lj} \quad (8)$$

This expression is similar to Eq. (7) (the only difference being the time variable T instead of T') and corresponds to dead time-free ESEEM along T because the measurements can be started from T = 0.

3.2. Interaction with several nuclei

Eqs. (1) and (2) actually represent sums of the traces of two matrices, one containing the terms with $\widetilde{T}_{\alpha ij}$, and the other containing the terms with $\widetilde{T}_{\beta ij}$:

$$V = \frac{1}{2}(V_\alpha + V_\beta) \quad (9)$$

where V_α and V_β correspond, respectively, to $\widetilde{T}_\alpha$ and $\widetilde{T}_\beta$, and we do not make a distinction between the RS and RV ESEEM. The numerical factor of 1/2 accounts for the standard normalization of V_α and V_β: $V_\alpha(0, 0, 0) = V_\beta(0, 0, 0) = 1$, where the arguments correspond to the three time intervals.

If the unpaired electron interacts with several magnetic nuclei, then each of the matrices entering V_α and V_β represents a Kronecker product of the matrices corresponding to the interactions with separate nuclei. From the well-known trace property of the Kronecker product, $\mathrm{Tr}(\mathbf{A}\otimes\mathbf{B}) = \mathrm{Tr}(\mathbf{A})\cdot\mathrm{Tr}(\mathbf{B})$, it then follows:

$$V = \frac{1}{2}\left(\prod_{i=1}^{N} V_{\alpha i} + \prod_{j=1}^{N} V_{\beta j}\right) \quad (10)$$

where N is the number of nuclei. This product rule is similar to that in stimulated ESEEM [39].

While in general the integral of a product is not equal to the product of integrals, one can show that for the integrated RV or RS ESEEM the product rule similar to Eq. (10) applies. Indeed, one can break V_α and V_β into two groups of terms, $V^{(\tau,t)}$ and $V^{(T)}$, similar to the grouping in Eqs. (4) and (5). The group $V^{(\tau,t)}$ contains the harmonics of τ and t that are averaged out by the integration, while $V^{(T)}$ contains the oscillations in T (or T') dimension that survive the integration. Then, in the case of two nuclei:

$$V_{\alpha(\beta)} = V_{\alpha(\beta)1}V_{\alpha(\beta)2} = \left(V^{(\tau,t)}_{\alpha(\beta)1} + V^{(T)}_{\alpha(\beta)1}\right)\left(V^{(\tau,t)}_{\alpha(\beta)2} + V^{(T)}_{\alpha(\beta)2}\right) = V^{(\tau,t)}_{\alpha(\beta)1}V^{(\tau,t)}_{\alpha(\beta)2} + V^{(\tau,t)}_{\alpha(\beta)1}V^{(T)}_{\alpha(\beta)2} + V^{(T)}_{\alpha(\beta)1}V^{(\tau,t)}_{\alpha(\beta)2} + V^{(T)}_{\alpha(\beta)1}V^{(T)}_{\alpha(\beta)2} \quad (11)$$

Integration over τ and t will eliminate the first three terms. The last term represents a product of the integrated ESEEMs from the two nuclei. Similar reasoning can be extended to arbitrary number of nuclei. Therefore, Eq. (10) is valid for the integrated RV and RS ESEEM.

3.3. Integrated RS and RV ESEEM for spin I = 1/2

From Eqs. (7) and (8) it is easy to obtain an explicit expression for the integrated RS and RV ESEEM in the case of I = 1/2. For example, the derivation for RV ESEEM gives:

$$\begin{aligned} V_{iRV} &= \frac{1}{2}(V_\alpha + V_\beta) \\ &= \frac{1}{2}\left(1 - \frac{k}{4}(3 - \cos(\omega_\alpha T))\right) \\ &\quad + \frac{1}{2}\left(1 - \frac{k}{4}(3 - \cos(\omega_\beta T))\right) \\ &= 1 - \frac{k}{8}(6 - \cos(\omega_\alpha T) - \cos(\omega_\beta T)) \end{aligned} \quad (12)$$

where k is the standard ESEEM amplitude factor:

$$k = \frac{\nu_I^2(T_{ZX}^2 + T_{ZY}^2)}{\nu_\alpha^2\nu_\beta^2} \quad (13)$$

In Eq. (13), T_{ij} are the components of the anisotropic *hfi* tensor, and axis Z corresponds to the direction of the external magnetic field, $\mathbf{B_o}$. The expression for V_{iRS} is obtained from Eq. (12) by substituting T by T'.

3.4. Experimental considerations

Let us consider now the essential points of the experimental design. To be efficient and practical, an experiment should not be excessively long. Already 2D experiments may take hours to finish. The RS and RV ESEEM experiments are potentially 3D, and it may seem that extremely long data acquisition time may be required to eventually obtain the desired 1D spectrum. Fortunately, however, this is not true, because we are only interested in averaging out the harmonics depending on τ and t. Therefore, the experiment

can be performed as 2D, with one dimension being T (or T'), and the other two time intervals being varied simultaneously in the second dimension. For example, Eq. (1) for RS ESEEM contains terms of both $\cos(\omega_T T + \omega_t t)$ and $(\omega_T T + \omega_\tau \tau)$ types, and thus both τ and t have to be varied in the "low-resolution" dimension. On the other hand, Eq. (2) for RV ESEEM does not contain terms of $\cos(\omega_T T + \omega_t t)$ type, and thus only τ needs to be varied in the "low-resolution" dimension, while t can be kept fixed.

Eq. (1) for V_{RS} is symmetric with respect to the interchange of τ and T' $\tau + T$. Therefore, the RS ESEEM experiment can be performed with a swapping of the second and third mw pulses (effectively, recording the ESEEM from $T < 0$), similar to the stimulated ESEEM [30]. In contrast to the stimulated ESEEM, however, in RS ESEEM T' can be made arbitrarily small without compromising the observability of the RS ESE signal. Therefore, by starting the sweeps in T dimension corresponding to different intervals τ from $T' \sim 0$ (*i.e.*, $T \sim -\tau$), one can obtain V_{iRS} with nearly zero dead time (there will actually be a residual dead time on the order of the mw pulse length; the same applies to V_{iRV}). The pulse swapping, however, introduces unrecoverable distortions into the RS ESEEM traces at $T = 0$ ($T' = \tau$) due to the collapse of the stimulated and RS ESE signals when the second and third pulses overlap. Although in the integrated RS ESEEM trace these distortions will be diminished, their presence imposes limitations on the applicability of RS ESEEM technique.

It follows from comparison of Eqs. (7) and (8) that the integrated RV ESEEM is formally equivalent to the integrated RS ESEEM. Its practical implementation, however, does not require pulse swapping, and the resulting integrated RV ESEEM is free from the pulse swapping artifacts. Therefore, in practical experiments the integrated RV ESEEM is to be preferred over the RS ESEEM, and we will only consider the integrated RV ESEEM below.

The last practical question we discuss here is related to the phase cycling. Under non-saturating conditions (*i.e.*, when pulse repetition rate is low compared with the electronic longitudinal relaxation rate), there is a total of 17 observable ESE signals formed by the pulse sequence of Fig. 1: six primary echoes (PE), four stimulated echoes (SE), four refocused primary echoes (RPE), one refocused refocused (double-refocused) primary echo (RRPE), one refocused stimulated echo (RSE) and one refocused virtual echo (RVE). Seven of these signals (namely, PE_{13}, PE_{23}, PE_{24}, SE_{134}, SE_{234}, RPE_{123}, and RPE_{124}, where the subscripts indicate the mw pulses forming the specific signal) may cross the RV ESE signal during the experiment, and their contribution has to be eliminated by a phase cycling. The minimal phase cycling that eliminates all of these unwanted echoes is shown in Table 1.

3.5. Experimental example

As an example, we present here the X-band ^{1}H ESEEM spectra of the molybdenum active center of SO, a ubiquitous enzyme that oxidizes toxic sulfite to sulfate. The Mo active center has an approximately square-pyramidal geometry, with four non-exchangeable ligands (one axial oxo, two equatorial sulfurs from pyranopterindithiolate cofactor, and one equatorial sulfur form a cysteinyl side chain) and one exchangeable equatorial ligand,

Table 1
Minimal phase cycle accumulating the RVE_{1234} signal and eliminating the unwanted PE_{13}, PE_{23}, PE_{24}, SE_{134}, SE_{234}, RPE_{123}, and RPE_{124} signals.

ϕ (mw_1)	ϕ (mw_2)	ϕ (mw_3)	ϕ (mw_4)	Operation on RVE_{1234}
0	0	0	0	+
π	0	0	0	−
0	π	0	0	−
π	π	0	0	+

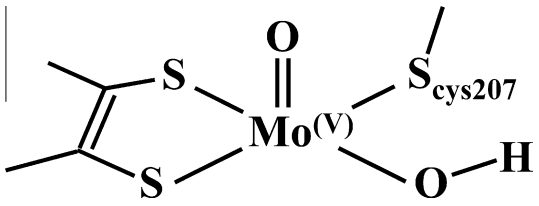

Fig. 2. The structure of the Mo(V) center of *lpH* SO. The OH bond of the OH ligand is approximately in the equatorial plane, which leads to strong *hfi* of the ligand proton. The cysteine ligand number corresponds to human SO.

which depends on the stage of the catalytic cycle and experimental conditions [40–42] (Fig. 2 schematically shows an example of the structure in the Mo(V) state discussed below).

The catalytic cycle starts with sulfite binding to the exchangeable equatorial oxo ligand of Mo(VI) and a two-electron reduction of the molybdenum to Mo(IV). The resulting equatorial sulfate ligand is then replaced by a hydroxyl, while the molybdenum is oxidized to Mo(V). The Mo(V) active center gives a readily detectable EPR signal, which depends on the buffer pH, organism, mutation, and presence of inhibiting anions in the media [37]. For example, the Mo(V) center of wild type vertebrate SO at low pH (<7) discussed here (so-called *lpH* form of SO) is characterized by the principal g-values of $(g_X, g_Y, g_Z) \approx (1.964, 1.972, 2.005)$ and doublet splittings $\sim$1 mT caused by the *hfi* with the OH ligand proton [38,43].

The isotropic and anisotropic *hfi* constants of the OH ligand proton were estimated by ^{1}H pulsed ENDOR ($a_{iso} \approx 26$ MHz; $T_\perp \approx -7$ MHz) [38] and ^{2}H ESEEM in the samples prepared in D_2O ($a_{iso} \approx 26$ MHz; $T_\perp \approx -5$ MHz, as recalculated from ^{2}H) [44],

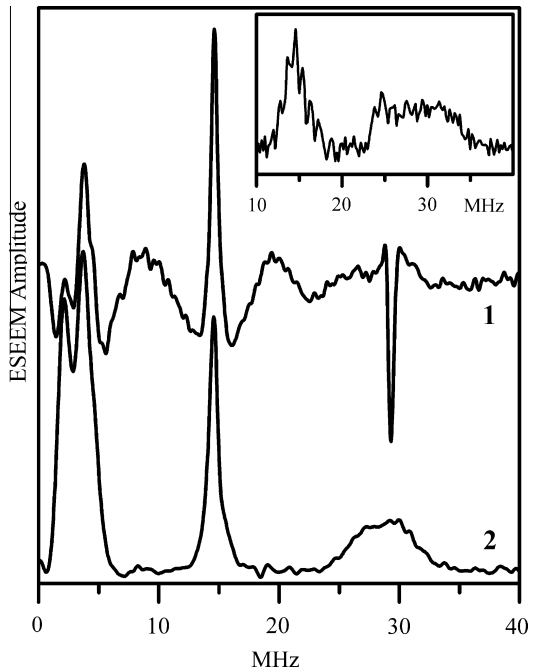

Fig. 3. The ESEEM spectra of human *lpH* SO (cosine FT) at the intermediate EPR turning point. Trace 1, two-pulse ESEEM spectrum. Trace 2, integrated RV ESEEM spectrum. Experimental conditions: mw frequency, 9.468 GHz; magnetic field, B_o = 3.430 mT; mw pulses, 10 ns and 15 ns for trace 1 and 3 × 10 ns and 15 ns for trace 2; temperature, 21 K. Inset: Davies ENDOR spectrum of human *lpH* SO recorded at the intermediate EPR turning point (see [38]. Experimental conditions: mw frequency, 9.446 GHz; B_o = 3.418 mT, mw pulses, 40 ns (180°), 20 ns (90°) and 40 ns (180°); time interval between the first and second mw pulses, 40 μs; time interval between the second and third mw pulses, 400 ns; rf pulse, 5 μs; temperature, 20 K).

but a direct observation of this proton by ^{1}H ESEEM presents a challenge because of the large width of the nuclear transition lines, $\Delta\nu \sim |3T_\perp/2| \sim 8$–10 MHz, which results in significant damping of the ESEEM within the dead time of 100–200 ns typical for the X-band experiments. In addition, in X-band experiments, the Zeeman – *hfi* cancellation condition ($\nu_H \sim A/2$, where ν_H is the ^{1}H Zeeman frequency) is realized for this proton, which results in an overlap of the high-frequency fundamental line ($\nu_\beta \approx \nu_H + A/2$) with the sum and difference combination lines ($\nu_\sigma \approx 2\nu_H$ and $\nu_\delta \approx A$, respectively).

As an example, trace 1 in Fig. 3 shows the primary ESEEM spectrum of human *lpH* SO obtained at the intermediate EPR turning point, g_Y. The prominent features in this spectrum are the fundamental line at $\nu_H \approx 14.6$ MHz and the sum combination line at $2\nu_H \approx 29.2$ MHz originating from weakly coupled protons. The ν_β fundamental line of the OH ligand proton occupying the range between about 24 and 34 MHz (as seen in pulsed ENDOR spectra [38]) is unobservable. For comparison, trace 2 in Fig. 3 shows the integrated RV ESEEM spectrum obtained under the same conditions. The lines of the OH ligand proton now are clearly seen. The high-frequency feature belongs to the OH ligand proton only, while the low-frequency one is also contributed to by the nearby chlorine nucleus [45]. This high-frequency part of the RV ESEEM spectrum is in good agreement with the Davies ENDOR spectrum recorded in similar conditions earlier [38] (Fig. 3 inset).

4. Conclusion

In this work we performed a theoretical analysis of RS and RV ESEEM techniques. This analysis revealed that integration of V_{RS} or V_{RV} over the two "low-resolution" time intervals, τ and t (or τ'), results in 1D ESEEM along T, which is free from dead time and blind spots, and phases uniformly in the cosine FT spectra. The practical implementation of V_{iRS} introduces artifacts related to the pulse swapping necessary to achieve the zero dead time. V_{iRV} does not require pulse swapping and is free from such artifacts, and it represents a robust practical technique for obtaining dead time- and blind spots-free spectra of fundamental lines.

Acknowledgments

The author is grateful to Prof. J.H. Enemark for making the sample of *lpH* SO available for this study, and to Dr. A.M. Raitsimring for stimulating discussions.

References

[1] S.A. Dikanov, Y.D. Tsvetkov, Electron Spin Echo Envelope Modulation (ESEEM) Spectroscopy, CRC Press, Boca Raton, 1992.
[2] A. Schweiger, G. Jeschke, Principles of Pulse Electron Paramagnetic Resonance, Oxford University Press, Oxford, 2001.
[3] W.B. Mims, K. Nassau, J.D. McGee, Spectral diffusion in electron resonance lines, Phys. Rev. 123 (1961) 2059–2069.
[4] D.E. Kaplan, M.E. Browne, J.A. Cowen, Pulsed X-band EPR spectrometer, Rev. Sci. Instrum. 32 (1961) 1182–1186.
[5] L.G. Rowan, E.L. Hahn, W.B. Mims, Electron-spin-echo envelope modulation, Phys. Rev. 137 (1965) 61–71.
[6] W.B. Mims, Envelope modulation in spin echo experiments, Phys. Rev. B 5 (1972) 2409–2419.
[7] W.B. Mims, Amplitudes of superhyperfine frequencies displayed in electron-spin-echo envelope, Phys. Rev. B 6 (1972) 3543–3545.
[8] A. Schweiger, Pulsed electron spin resonance spectroscopy: basic principles, techniques, and examples of applications, Angew. Chem., Int. Ed. Engl. 30 (1991) 265–292.
[9] S. Van Doorslayer, A. Schweiger, A two-dimensional sum combination frequency pulse epr experiment, Chem. Phys. Lett. 281 (1997) 297–305.
[10] P. Höfer, A. Grupp, H. Nebenführ, M. Mehring, Hyperfine sublevel correlation (HYSCORE) spectroscopy: a 2D ESR investigation of the squaric acid radical, Chem. Phys. Lett. 132 (1986) 279–282.
[11] A.V. Astashkin, A.M. Raitsimring, Refocused primary echo: a zero dead time detection of the electron spin echo envelope modulation, J. Magn. Reson. 143 (2000) 280–291.
[12] A.V. Astashkin, S.A. Dikanov, Y.D. Tsvetkov, Spectrometer dead time: effect on electron spin echo modulation spectra in disordered systems, Chem. Phys. Lett. 136 (1987) 204–208.
[13] S.A. Dikanov, A.V. Astashkin, Y.D. Tsvetkov, Elimination of the matrix contribution to electron spin echo modulation, Chem. Phys. Lett. 144 (1988) 251–257.
[14] A.V. Astashkin, M.L. Mader, A. Pacheco, J.H. Enemark, A.M. Raitsimring, Direct detection of the proton-containing group coordinated to Mo(V) in the high pH form of chicken liver sulfite oxidase by refocused primary ESEEM spectroscopy: structural and mechanistic implications, J. Am. Chem. Soc. 122 (2000) 5294–5302.
[15] A.V. Astashkin, F. Neese, A.M. Raitsimring, J.J.A. Cooney, E. Bultman, J.H. Enemark, Pulsed EPR investigations of systems modeling molybdenum enzymes: hyperfine and quadrupole parameters of Oxo-^{17}O in $[Mo^{17}O(SPh)_4]^-$, J. Am. Chem. Soc. 127 (2005) 16713–16722.
[16] S.A. Dikanov, Y.D. Tsvetkov, M.K. Bowman, A.V. Astashkin, Parameters of quadrupole coupling of ^{14}N nuclei in chlorophyll a cations determined by the electron spin echo method, Chem. Phys. Lett. 90 (1982) 149–153.
[17] Y. Deligiannakis, A. Boussac, W. Rutherford, ESEEM study of the plastoquinone anion radical (Q_A^-) in ^{14}N- and ^{15}N-labeled photosystem II treated with CN, Biochemistry 34 (1995) 16030–16038.
[18] A.V. Astashkin, A. Kawamori, Y. Kodera, S. Kuroiwa, K. Akabori, An electron spin echo envelope modulation study of the primary acceptor quinone in Zn-substituted plant photosystem II, J. Chem. Phys. 102 (1995) 5583–5588.
[19] E. Aronoff-Spencer, C.S. Burns, N.I. Avdievich, G.J. Gerfen, J. Peisach, W.E. Antholine, et al., Identification of the Cu^{2+} binding sites in the N-terminal domain of the prion protein by EPR and CD spectroscopy, Biochemistry 39 (2000) 13760–13771.
[20] S.A. Dikanov, D.R.J. Kolling, B. Endeword, R.I. Samoilova, T.F. Prisner, S.K. Nair, et al., Identification of hydrogen bonds to the Rieske cluster through the weakly coupled nitrogens detected by electron spin echo envelope modulation spectroscopy, J. Biol. Chem. 281 (2006) 27416–27425.
[21] J. McCracken, I.R. Vassiliev, E. Yang, K. Range, B.A. Barry, ESEEM studies of peptide nitrogen hyperfine coupling in tyrosyl radicals and model peptides, J. Phys. Chem. B 111 (2007) 6586–6592.
[22] G.J. Yeagle, M.L. Gilchrist, R.M. McCarrick, R.D. Britt, Multifrequency pulsed electron paramagnetic resonance study of the S_2 state of the photosystem II manganese cluster, Inorg. Chem. 47 (2008) 1806–1814.
[23] L. Sun, J. Hernandes-Guzman, K. Warncke, OPTESIM, a versatile toolbox for numerical simulation of electron spin echo envelope modulation (ESEEM) that features hybrid optimization and statistical assessment of parameters, J. Magn. Reson. 200 (2009) 21–28.
[24] P.J. Alonso, J. Antorrena, J.I. Martinez, J.J. Novoa, F. Palacio, J.M. Rawson, et al., A CW-EPR and ESEEM spectroscopic study of the dithiadiazolyl radicals p-XC_6F_4CNSSN (X = CN, Br), Appl. Magn. Reson. 20 (2001) 231–247.
[25] A.V. Astashkin, K. Johnson-Winters, E.L. Klein, R.S. Byrne, R. Hille, A.M. Raitsimring, et al., Direct demonstration of the presence of coordinated sulfate in the reaction pathway of arabidopsis thaliana sulfite oxidase using ^{33}S labeling and ESEEM spectroscopy, J. Am. Chem. Soc. 129 (2007) 14800–14810.
[26] A.V. Astashkin, K. Johnson-Winters, E.L. Klein, C. Feng, H.L. Wilson, K.V. Rajagopalan, et al., Structural studies of the molybdenum center of the pathogenic R160Q mutant of human sulfite oxidase by pulsed EPR spectroscopy and ^{17}O and ^{33}S labeling, J. Am. Chem. Soc. 130 (2008) 8471–8480.
[27] P. Hoefer, Distortion-free electron-spin-echo envelope-modulation spectra of disordered solids obtained from two- and three-dimensional HYSCORE experiments, J. Magn. Reson. A 111 (1994) 77–86.
[28] A.V. Astashkin, A.M. Raitsimring, Properties of the HYSCORE spin echo signal, J. Magn. Reson. 148 (2001) 379–387.
[29] A.V. Astashkin, E.L. Klein, D. Ganyushin, K. Johnson-Winters, F. Neese, U. Kappler, et al., Exchangeable oxygens in the vicinity of the molybdenum center of the high-pH form of sulfite oxidase and sulfite dehydrogenase, Phys. Chem. Chem. Phys. 11 (2009) 6733–6742.
[30] J. Fauth, A. Schweiger, L. Braunschweiler, J. Forrer, R.R. Ernst, Elimination of unwanted echoes and reduction of dead time in three-pulse electron spin-echo spectroscopy, J. Magn. Reson. 66 (1986) 74–85.
[31] A.L. Bloom, Nuclear induction in inhomogeneous fields, Phys. Rev. 98 (1950) 1105–1111.
[32] P.E. Doan, B.M. Hoffman, Making hyperfine selection in Mims ENDOR independent of deadtime, Chem. Phys. Lett. 269 (1997) 208–214.
[33] L.V. Kulik, Y.A. Grishin, S.A. Dzuba, I.A. Grigoryev, S.V. Klyatskaya, S.F. Vasilevsky, et al., Electron dipole–dipole ESEEM in field-step ELDOR of nitroxide biradicals, J. Magn. Reson. 157 (2002) 61–68.
[34] A.V. Astashkin, J. Seravalli, S.O. Mansoorabadi, G.H. Reed, S.W. Ragsdale, Pulsed electron paramagnetic resonance experiments identify the paramagnetic intermediates in the pyruvate ferredoxin oxidoreductase catalytic cycle, J. Am. Chem. Soc. 128 (2006) 3888–3889.
[35] A.V. Astashkin, B.O. Elmore, W. Fan, J.G. Guillemette, C. Feng, Pulsed EPR determination of the distance between heme iron and FMN centers in a human inducible nitric oxide synthase, J. Am. Chem. Soc. 132 (2010) 12059–12067.
[36] A.V. Astashkin, J.H. Enemark, A.M. Raitsimring, 26.5–40 GHz K_a-Band pulsed EPR spectrometer, Concepts Magn. Reson., B 29B (2006) 125–136.
[37] J.H. Enemark, A.V. Astashkin, A.M. Raitsimring, High-resolution EPR spectroscopy of Mo enzymes. Sulfate oxidases: structural and functional

implications, in: G. Hanson, L. Berliner (Eds.), Metals in Biology: Applications of High Resolution EPR to Metalloenzymes, Springer, New York, 2010, pp. 121–168.
[38] A.V. Astashkin, A.M. Raitsimring, C. Feng, J.L. Johnson, K.V. Rajagopalan, J.H. Enemark, The Mo-OH proton of the low-pH form of sulfate oxidase: comparison of the hyperfine interactions obtained from pulsed ENDOR, CW-EPR and ESEEM measurements, Appl. Magn. Reson. 22 (2002) 421–430.
[39] S.A. Dikanov, A.A. Shubin, V.N. Parmon, Modulation effects in the electron spin echo resulting from hyperfine interaction with a nucleus of an arbitrary spin, J. Magn. Reson. 42 (1981) 474–487.
[40] C. Kisker, H. Schindelin, A. Pacheco, W.A. Wehbi, R.M. Garrett, K.V. Rajagopalan, et al., Molecular basis of sulfite oxidase deficiency from the structure of sulfite oxidase, Cell 91 (1997) 973–983.
[41] N. Schrader, K. Fischer, K. Theis, R.R. Mendel, G. Schwarz, C. Kisker, The crystal structure of plant sulfite oxidase provides insights into sulfite oxidation in plants and animals, Structure 11 (2003) 1251–1263.
[42] U. Kappler, S. Bailey, Molecular basis of intramolecular electron transfer in sulfite-oxidizing enzymes is revealed by high resolution structure of a heterodimeric complex of the catalytic molybdopterin subunit and a c-type cytochrome subunit, J. Biol. Chem. 280 (2005) 24999–25007.
[43] M.T. Lamy, S. Gutteridge, R.C. Bray, Electron-paramagnetic-resonance parameters of molybdenum(V) in sulphite oxidase from chicken liver, Biochem. J. 185 (1980) 397–403.
[44] A.M. Raitsimring, A. Pacheco, J.H. Enemark, ESEEM investigations of the high pH and low pH forms of chicken liver sulfite oxidase, J. Am. Chem. Soc. 120 (1998) 11263–11278.
[45] E.L. Klein, A.V. Astashkin, D. Ganyushin, C. Riplinger, K. Johnson-Winters, F. Neese, et al., Direct detection and characterization of chloride in the active site of the low-pH form of sulfite oxidase using electron spin echo envelope modulation spectroscopy, isotopic labeling, and density functional theory calculations, Inorg. Chem. 48 (2009) 4743–4752.